Journal of African Earth Sciences xxx (2014) xxx–xxx

Contents lists available at ScienceDirect

Journal of African Earth Sciences

journal homepage: www.elsevier.com/locate/jafrearsci

Integrating geologic and satellite radar data for mapping dome-and-basin patterns in the In Ouzzal Terrane, Western Hoggar, Algeria

Jean-Paul Deroin [a,*], Safouane Djemai [b], Abderrahmane Bendaoud [b], Boualem Brahmi [b], Khadidja Ouzegane [b], Jean-Robert Kienast [c]

[a] Université de Reims Champagne-Ardenne, Faculty of Science, EA 3795 GEGENAA – FR CNRS 3417 Condorcet, 2 esplanade Roland Garros, 51100 Reims, France
[b] LGGIP/FSTGAT/USTHB, BP. 32, El Alia, Bab Ezzouar, Alger 16111, Algeria
[c] Institut de Physique du Globe de Paris, IPGP, 4 place Jussieu, 75252 Paris cedex 05, France

ARTICLE INFO

Article history:
Received 30 July 2013
Received in revised form 5 March 2014
Accepted 14 March 2014
Available online xxxx

Keywords:
Geological mapping
Radar
Archaean
Dome-and-basin
In Ouzzal

ABSTRACT

The In Ouzzal Terrane (IOT) located in the north-western part of the Tuareg Shield forms an elongated N–S trending block, more than 400 km long and 80 km wide. It involves an Archaean crust remobilized during a very high-temperature metamorphic event related to the Palaeoproterozoic orogeny. The IOT largely crops out in the rocky and sandy desert of Western Hoggar. It corresponds mainly to a flat area with some reliefs composed of Late Panafrican granites, dyke networks or Cambrian volcanic rocks. These flat areas are generally covered by thin sand veneers. They are favorable for discriminating bedrock geological units using imaging radar, backscattering measurements, and field checking, because the stony desert is particularly sensitive to the radar parameters such as wavelength or polarization. The main radar data used are those obtained with the ALOS-PALSAR sensor (L-band), in ScanSAR mode (large swath) and Fine Beam modes. The PALSAR sensor has been also compared to ENVISAT-ASAR and to optical imagery.

Detailed mapping of some key areas indicates extensive Archaean dome-and-basin patterns. In certain parts, the supracrustal synforms and orthogneiss domes exhibit linear or circular features corresponding to shear zones or rolling structures, respectively. The geological mapping of these dome-and-basin structures, and more generally of the Archaean and Proterozoic lithological units, is more accurate with the SAR imagery, particularly when using the L-band, than with the optical imagery. A quantitative approach is carried out in order to estimate the backscatter properties of the main rock types. Due to the large variety of configurations, radar satellite imagery such as ALOS PALSAR represents a key tool for geological mapping in arid region at different scales from the largest (e.g., 1:500,000) to the smallest (e.g., 1:50,000).

1. Introduction

In arid regions where only reconnaissance geological maps exist, remote sensing is known to represent the cheapest and efficient way to compile geological maps. In these regions, morphologies are particularly well expressed and it is relatively easy to follow the geological boundaries on large distance. Typical morphologies occur, especially in the Saharan desert. Rock surfaces are more or less rough (reg surfaces) and frequently invaded by sand (serir surfaces). Radar can penetrate dry sand and image shallow sub-surface features (Abdelsalam et al., 2000). Fig. 1 illustrates the complementarity of radar and optical images in arid regions. The main advantage of the radar for geological mapping is to be less sensitive than optical data to sand cover (A is a dune clearly visible on the optical image) and hydrographic network (B is a wadi too flat and smooth to modulate the radar signal), and to be more sensitive to surface roughness (see D). The radar generally emphasizes dykes and prominent outcrops (see C), but incidence angle conditions play an important role. Note that the incidence angle is defined as the angle between the normal to the surface and the incident ray. Experiments show that the SAR signal is attenuated to about 40% at the air/sand interface and completely attenuated

* Corresponding author. Tel.: +33 3 26 91 33 76.
E-mail addresses: jean-paul.deroin@univ-reims.fr (J.-P. Deroin), safouane.djemai@gmail.com (S. Djemai), abendaoud@gmail.com (A. Bendaoud), boualem.brahmi@gmail.com (B. Brahmi), k.ouzegane@gmail.com (K. Ouzegane), jeanrobert.kienast@gmail.com (J.-R. Kienast).

http://dx.doi.org/10.1016/j.jafrearsci.2014.03.015
1464-343X/

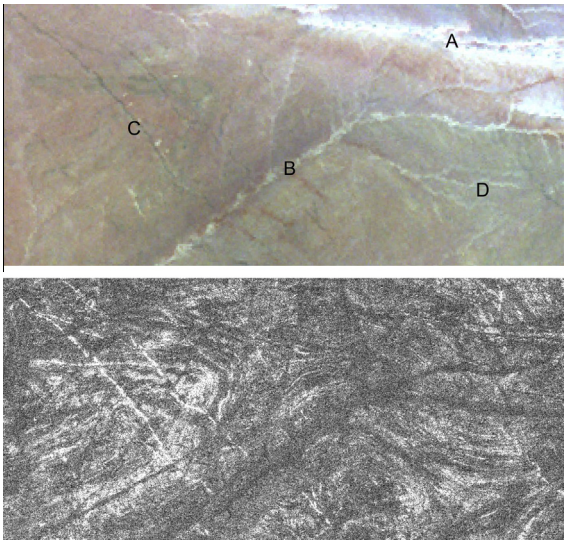

Fig. 1. Comparison of optical and radar data in arid region. Example of the Abeleyel area (see text for explanation).

at depth more than 2 m at 1% moisture content (Elachi and Granger, 1982).

The Hoggar is composed of well preserved and largely reworked Archaean (3200–2500 Ma) and Palaeoproterozoic terranes (2000 Ma) and juvenile Pan-African terranes (750–550 Ma) (Caby, 2003; Ouzegane et al., 2003b). The In Ouzzal area is known as one of the Archaean terranes. It is embedded between the West African Craton and the Saharan Metacraton. The size, remoteness, and inhospitable character of the area induce difficulties for field work. In this context optical remote sensing has been successfully tested by Djemai (2008). Now, the second step consists in evaluating radar data, particularly to focus on key areas in the heart of In Ouzzal Terrane, particularly those representing hypothesized dome-and-basin structures (Ouzegane et al., 2003b). The present paper emphasizes the results obtained mainly with the ALOS PALSAR data.

2. History of space borne imaging radar

The history of satellite imaging radar goes back to 1978 when SEASAT, carrying the first Synthetic Aperture Radar (SAR) instrument, was launched. SAR techniques have been widely used for various applications, including geological mapping in arid regions. With its 105 day-life the SEASAT mission provides seminal geological radar studies (Elachi et al., 1985; Deroin et al., 1991; Evans et al., 2005). The specific interest of radar remote sensing in arid subsurface studies has been illustrated in the Eastern Sahara, Egypt, from the SIR-A and SIR-B missions (McCauley et al., 1982; Schaber et al., 1986). These studies particularly revealed palaeodrainage channels along the Nile valley using the potential for penetrating sand veneer (McCauley et al., 1986; Schaber and Breed, 1999). The potential for geological mapping has been less frequently evaluated, but is known to be better when large wavelengths are used (Schaber et al., 1997). Radar bands used in satellite SAR systems have wavelengths such as about 3 cm for the X-band, about 6 cm for the C-band, about 10 cm for the S-band, and 24 cm for the L-band (Table 1). Note that the longer wavelengths corresponding to the so-called P-band at about 60 cm are only utilizable on board airborne vectors such as the AIRSAR (Schaber, 1999; Daniels et al., 2003).

The interest of SAR remote sensing increased in the early 1990s. After the seminal but limited SAR missions of the American SEASAT in 1978 and the Soviet ALMAZ in 1987–1989, SAR imagery became more common in geological studies with the successive launches of ERS-1 in 1991, JERS-1 in 1992, and ERS-2 and RADARSAT-1 in 1995, all in single polarization (Chorowicz et al., 2005). In 1994 NASA twice launched the Shuttle Endeavour in the frame of the SIR-C/X-SAR mission to collect multi-look angles and swaths data (Evans et al., 1997). The SIR-C/X-SAR data were simultaneously collected at three wavelengths (X, C, and L-band) and multiple polarizations. Geological applications show that the L-band is always preferable to the C-band (Schaber and Breed, 1999; Abdelsalam et al., 2000), and that a relatively high incident angle (35–50°) is required to avoid geometric distortion and lay-over problems, and to obtain deeper penetration (Rudant et al., 1994; Inzana et al., 2003; Raharimahefa and Kusky, 2006). However, some studies indicated that the C-band is also suitable for identifying surface roughness of relatively smooth surfaces in flat areas (Deroin et al., 1997, 1998; Singhroy, 2001; Thurmond et al., 2006; Pal et al., 2007). SARs on board ERS-2 and ENVISAT (ASAR) are similar to the one on board ERS-1. ALOS launched in 2006 represents the major advance in radar remote sensing for geological mapping. The radar sensor, the so called PALSAR, is able to acquire data in different modes (see also Section 3) and allows to develop interferometric applications (Chaussard et al., 2013).

Table 1
The SAR s/c systems and their main characteristics. ASI (Italian Space Agency), CSA (Canadian Space Agency), DLR (German Space Agency), ESA (European Space Agency), JAXA (Japanese Space Agency), NASA (US Space Agency), RSA (Russian Space Agency).

Satellite	Sensor (agency)	Mission	Band	Incident angle	Resolution (m)	Polarization
SEASAT	SAR (NASA)	1978–1978	L	20°	25	HH
Shuttle	SIR-A (NASA)	1981–1981	C	45°	30	HH
	"		L	"	30	HH
Shuttle	SIR-B (NASA)	1984–1984	C	15–55°	30	HH
	"		L	"	30	HH
COSMOS-1870	EKOR (RSA)	1987–1989	S	30–60°	15	HH
ALMAZ-1	EKOR-A (RSA)	1991–1992	S	30–60°	15	HH
ERS 1	EMI (ESA)	1991–2000	C	23°	25	VV
JERS 1	SAR (JAXA)	1992–1998	L	35°	18	HH
Shuttle	X-SAR (DLR)	1994–1994	X	20–65°	25	VV
	SIR-C (NASA)	"	C	"	25	All
	SIR-C (NASA)	"	L	"	25	All
ERS 2	EMI (ESA)	1995–2011	C	23°	25	VV
RADARSAT 1	SAR (CSA)	1995–2013	C	17–50°	10–100	HH
ENVISAT	ASAR (ESA)	2002–2012	C	23–45°	25	HH, VV
ALOS 1	PALSAR (JAXA)	2006–2011	L	10–60°	10–100	HH, VV, HV, VH
TERRA SARX	SAR (DLR)	2006-present	X	60° max	1–18	HH, VV or HV-VH
COSMOSkyMed	SAR2000 (ASI)	2007-present	X	60° max	1–100	HH, VV or HV-VH
RADARSAT 2	SAR (CSA)	2007-present	C	17–59°	10–100	HH, VV, HV, VH
TanDEM-X	SAR (DLR)	2010-present	X	60° max	1–18	HH, VV, HV, VH

Please cite this article in press as: Deroin, J.-P., et al. Integrating geologic and satellite radar data for mapping dome-and-basin patterns in the In Ouzzal Terrane, Western Hoggar, Algeria. J. Afr. Earth Sci. (2014), http://dx.doi.org/10.1016/j.jafrearsci.2014.03.015

Fig. 2. Location of In Ouzzal, southern Algeria, in northern Africa.

Radar remote sensing is frequently combined with optical remote sensing (Kusky and Ramadan, 2002; Gani and Abdelsalam, 2006; Brahmi et al., 2012). Remote sensing can be used together with geophysical data, either when optical data (Chernicoff and Nash, 2002) or radar data (Deroin and Delor, 2010) are concerned. Data fusion is generally used. Both remote sensing and geophysical data are then merged using a geographic information system (GIS).

3. Study site

The remote In Ouzzal area is located in southern Algeria, about 300 km to the west of Tamanrasset (Fig. 2). The In Ouzzal Terrane (IOT), also known as In Ouzzal Granulitic Unit (IOGU), forms an elongated N–S trending block, 450 km long and 70–80 km wide. The norther part of IOT (22°50′-23°30′N–2°20′-3°20′W) was investigated in the present study (Fig. 3). Main relief rising several hundreds of meters above the In Ouzzal granulitic reg (average elevation at about 500 m above sea level) is made of Cambrian ignimbrite massifs, and Pan-African granites of In Hihaou and In Eher in the West, Nahalet and Tihimatine in the centre, and Ihouhaouene in the East (Fig. 3).

Denaeyer (1934) identified granulitic rocks in this part of the north-western Tuareg Shield, which is composed of terranes welded together during the Pan-African orogeny (Black et al., 1994). Then, Lelubre (1952) described the petrological nature of the rocks and compared them to the famous charnockites of India. Lelubre's seminal works lead to the first large-scale geological map of the area, stressing steeply dipping foliations, the direction of which is modified in the neighbourhood of the Pharusian (Neoproterozoic) terranes. In the 1960s, several field works conducted in the northern part of the In Ouzzal area (Giraud, 1961; Gravelle, 1969) helped to draw synthetical geological maps of the Hoggar (Reboul et al., 1962; Caby and Bertrand, 1977). These authors also identified a granulitic complex composed of charnockites, garnet–graphite gneisses, nodular marbles, and different types of quartzites. The first

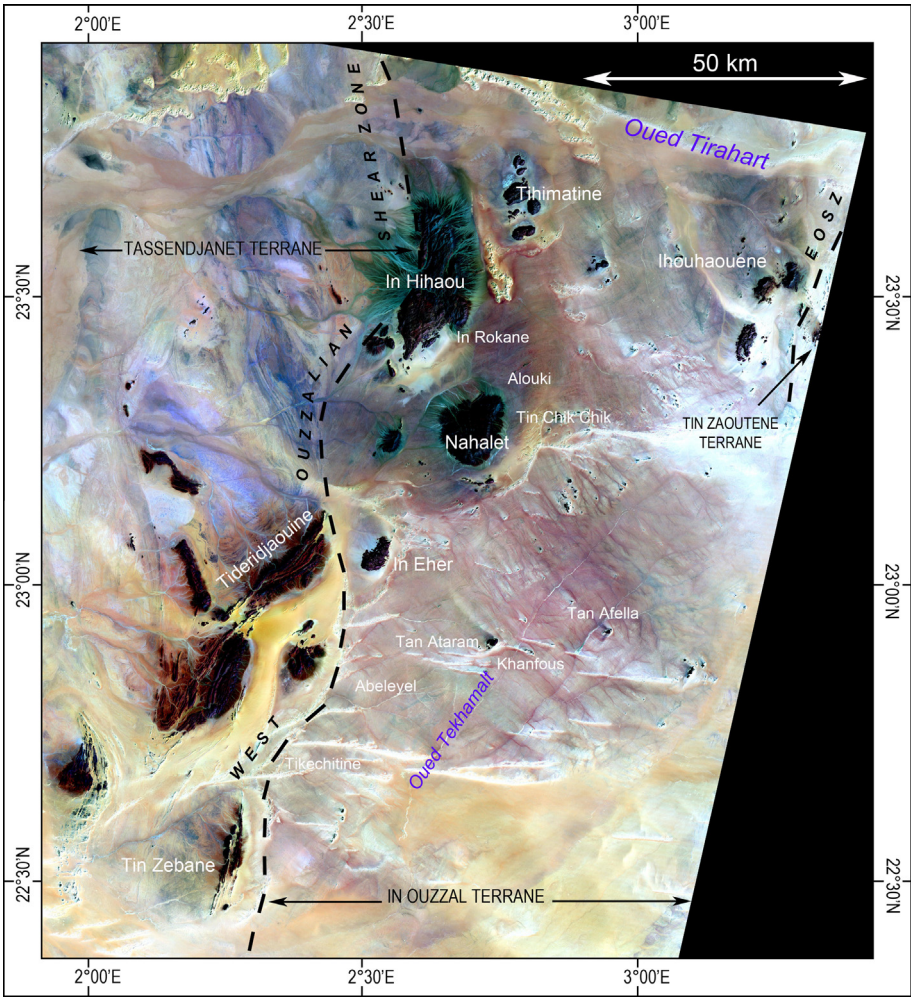

Fig. 3. The In Ouzzal Terrane. Landsat TM data acquired on 3rd March 1987. Color composite: red = band 7(SWIR range), green = band 3 (red range), blue = band 1 (blue range). EOSZ. East Ouzzalian Shear Zone. (For interpretation of the references to color in this figure legend, the reader is referred to the web version of this article.)

Please cite this article in press as: Deroin, J.-P., et al. Integrating geologic and satellite radar data for mapping dome-and-basin patterns in the In Ouzzal Terrane, Western Hoggar, Algeria. J. Afr. Earth Sci. (2014), http://dx.doi.org/10.1016/j.jafrearsci.2014.03.015

Archaean age (2995 Ma total rock Rb/Sr date) is reported by Ferrara and Gravelle (1966) and confirmed by others (Allègre and Caby, 1972; Lancelot et al., 1976; Ben Othman et al., 1984; Haddoum et al., 1994; Peucat et al., 1996). It is now generally accepted that two Archaean units are present in the IOT; a 3.2–2.7 Ga orthogneiss and charnockite unit (Haddoum et al., 1994) and a metasediment unit composed of marbles, quartzite and Al–Mg and Al–Fe granulites (Bernard-Griffiths et al., 1996; Djemai, 2008).

Single mineral datings (U-Pb zircon, Nd-Sr, etc.) show more recent dates ranging from 2100 Ma to 1950 Ma, interpreted as the

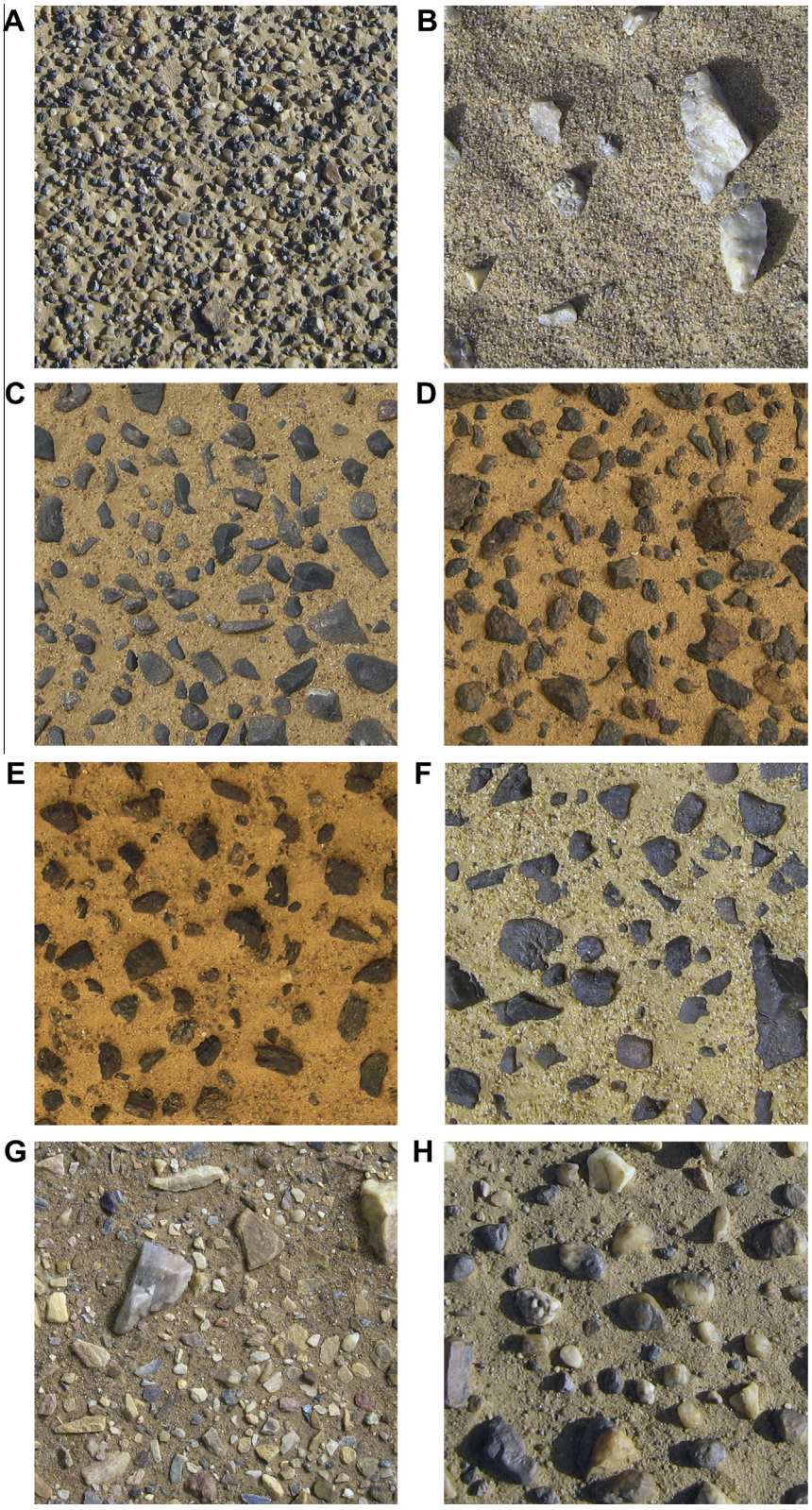

Fig. 4. Examples of reg surfaces in the In Ouzzal area. Each photograph covers exactly 20 cm × 20 cm. Nature of the substrate. (A) Water-borne deposits (fine). (B) Granite (note the broken quartz chips). (C) Dolerites. (D) Quartz with magnetite. (E) Banded iron formations. (F) Black quartzite with sand (serir). (G) Quartzite. (H) Water-borne deposits (rough).

Please cite this article in press as: Deroin, J.-P., et al. Integrating geologic and satellite radar data for mapping dome-and-basin patterns in the In Ouzzal Terrane, Western Hoggar, Algeria. J. Afr. Earth Sci. (2014), http://dx.doi.org/10.1016/j.jafrearsci.2014.03.015

remobilization of the Archaean crust during a very high-temperature (⩽1100 °C; 10–11 kbar) metamorphic event related to the Palaeoproterozoic Eburnean orogeny dated to ~2.1 Ga (Kienast and Ouzegane, 1987; Black et al., 1994; Caby, 1996; Ganne et al., 2014). Some mineral parageneses confirm these extreme temperature conditions, e.g. marbles with wollastonite–scapolite–calcite–quartz, anorthite–grossularite (Ouzegane et al., 2003a) or the spinel–quartz quartzites with or without corundum (Guiraud et al., 1996). Two major syntheses were published in the form of special issues on the In Ouzzal granulite unit (Kienast et al., 1996), and on the Precambrian of the Hoggar massif (Ouzegane et al., 2003c), respectively.

The Archaean IOT is composed of two units dated to 3.5–2.7 Ga (Lancelot et al., 1976; Ben Othman et al., 1984; Peucat et al., 1996). The lower crustal unit is made up essentially of charnockites and enderbites. The supracrustal unit comprises quartzites, marbles, banded iron formations (BIF), Al–Mg and Al–Fe granulites commonly associated with mafic and ultramafic lenses. Alumino–magnesian granulites are generally rich in quartz but sometimes they are quartz-free and then rich in sapphirine providing a typical blue color in the field. Al–Mg granulites are well developed in the northern part of In Ouzzal, near Adrar In Hihaou and Oued Tekhamalt. These granulites are also in contact with metaigneous rocks such as charnockites, enderbites, metanorites or peridotites. The torsion of orthopyroxene cleavage planes and garnet or orthopyroxene porphyroblasts show a ductile behavior expressed by an elongation of the grains and provide evidence of high-temperature deformation. All these rocks present the orthopyroxene–sillimanite association along with a diverse mineralogy made up of cordierite, biotite, spinel, corundum, plagioclase, potassic feldspar, ilmenite and rutile (Ouzegane, 1987; Kienast and Ouzegane, 1987).

Boundaries between In Ouzzal Terrane and branches of the Pan-African belt are represented by vertical wrench faults. The IOT has been preserved during the Pan-African orogeny, during which it behaved as a relatively rigid body. The East-In Ouzzal mylonitic margin (or East Ouzzalian Shear Zone) was studied in detail in the southern part of the IOT near Amesmessa, 200 km to the south of Tin Zebane (Djemai, 1996), where it consists of a major vertical fault with a dextral strike-slip component. On the contrary, the West-Ouzzalian Shear Zone indicates a sinistral displacement

Table 2
ALOS scenes acquired over the In Ouzzal test site.

Sensor	Mode	Date of acq.	Resolution (m)	Surface (km × km)	Orbit
Radar images					
PALSAR	ScanSAR	2009 02 25	100	350 × 330	Descending
PALSAR	QUAD-POL	2007 05 27	12.5	24 × 8	Ascending
PALSAR	FSB	2010 04 24	6.25	70 × 70	Ascending
Optical images					
AVNIR-2 (north)		2008 08 06	10	70 × 70	Descending
AVNIR-2 (south)		2008 08 06	10	70 × 70	Descending
PRISM (Tin Zebane)		2008 09 21	2.5	35 × 35	Descending
PRISM (Tan Ataram)		2009 10 23	2.5	35 × 35	Descending

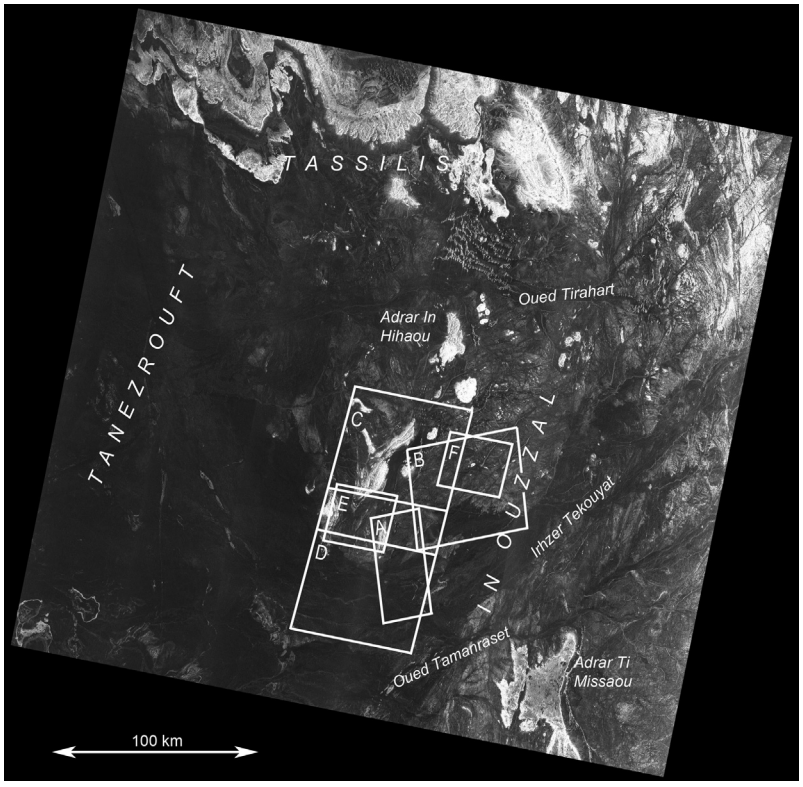

Fig. 5. The Hoggar region as seen with ALOS PALSAR (ScanSAR mode) and position of the ALOS scenes acquired in the frame of the pilot project. A (Polarimetry mode), B (Fine Beam Single mode), C–D (AVNIR-2 mode), E–F (PRISM mode).

Please cite this article in press as: Deroin, J.-P., et al. Integrating geologic and satellite radar data for mapping dome-and-basin patterns in the In Ouzzal Terrane, Western Hoggar, Algeria. J. Afr. Earth Sci. (2014), http://dx.doi.org/10.1016/j.jafrearsci.2014.03.015

(Caby, 1970), the last movements along the fault occurring simultaneously with the emplacement of the Tin Zebane alkaline–peralkaline dyke swarm (Hadj-Kaddour et al., 1998; Ait-Djafer et al., 2003). A deeply rooted fault has been suggested by Bouzid et al. (2008) using magnetotelluric measurements. It may be interpreted as a major fault that separates IOT into two compartments.

Due to the climate conditions, the surface of the stony desert corresponds to the reg, a typical gravel veneer, normally consisting of small, round or flat pebbles, characterizing extensive desert plain from which fine sand has been removed by the wind. Typical pavements such as in the flat areas of the Adrar plateau, Mauritania (Deroin et al., 1998) are relatively rare. The geological deposits are alluviums, eolian sands, smooth or gravelly reg, veneer of mixed sand and gravel (serir), and rock slabs. Fig. 4 illustrates typical surfaces observed in the field in the In Ouzzal Terrane.

4. Methods

4.1. Principle

Spaceborne imaging radar is unique in geological remote sensing because it is an active system that uses electromagnetic signals with centimetric microwaves and systems with side-looking geometry. Basically, the radar impulse response or backscattering is modulated by three geometrical and dielectric parameters, i.e., slope, humidity, and roughness of the land surface. When flat areas are under investigation, soil roughness and soil moisture are main factors, as shown individually by experimentation and modelling studies (Evans et al., 1992; Archer and Wadge, 2001; Deroin et al., 1997; Rémond and Deroin, 1997; Paillou et al., 2003). In an arid test site, humidity can be considered as constant (and very low). Furthermore, if flat areas are chosen, only surface roughness significantly modulates the radar response.

4.2. SAR imagery

4.2.1. ALOS data

The ALOS satellite was launched from Tanegashima Space Center, Japan, on 24 January 2006 (Rosenqvist et al., 2007). The satellite was placed in a near-polar orbit at 691 km, with a local equator pass time at about 10:30 (morning descending pass) and 22:30 (evening ascending pass), respectively. A short time after its 5th anniversary, it was declared dead in orbit after abruptly powering down on 22 April. ALOS 2 is expected to be launched in 2014. ALOS carried three sensors: (i) the Panchromatic Remote-Sensing Instrument for Stereo Mapping (PRISM), a panchromatic radiometer working in the range 520–770 nm, with 2.5-m spatial resolution; (ii) the Advanced Visible and Near-Infrared Radiometer type 2 (AVNIR-2), a multispectral radiometer with 10-m ground resolution and four spectral bands in the visible and near infrared range, and (iii) the Phased Array L-band Synthetic Aperture Radar (PALSAR).

PALSAR is a fully polarimetric instrument, which operates in L-band ($\lambda = 23.6$ cm). It can be operated in different observation modes including: Fine Beam Single polarization (FBS), Fine Beam Dual polarization (FBD), Polarimetric mode (POL), and the scanning mode (ScanSAR). Different ALOS data were obtained in the frame of a pilot project of the Japanese Space Agency (JAXA) and the European Space Agency (ESA) (Table 2). The cover of each ALOS scene is summarized in Fig. 5. In the present paper, the FBS and ScanSAR modes were mainly evaluated.

Single polarization available with fine beam modes is horizontally transmitted, horizontally received (HH). The pixel size is 6.25 m in FBS mode, corresponding to a nominal resolution of 10 m. ScanSAR mode is also horizontally transmitted horizontally received (HH), but the pixel size is 100 m.

For PALSAR products (level 1.5) used in this study, the conversion between the digital number (DN) of the amplitude image and the backscattering expressed by the sigma-naught (σ^0) at nominal incident angle is given by Eq. (1) (Shimada et al., 2009):

$$\sigma^0 = 10.\log_{10}[DN^2] + CF \quad (1)$$

where CF is the conversion factor. CF = −83.4 for FBS data acquired with an incident angle of 34.3°, and CF = −83 for ScanSAR data.

4.2.2. ASAR

ENVISAT was launched from Kourou Space Center, French Guiana, on 28 February 2002 (Desnos et al., 2000). ESA formally announced the end of ENVISAT's mission on 9 May 2012, one month after losing contact. ENVISAT was placed in a near-polar orbit at 790 km altitude. It was designed to study many processes of the

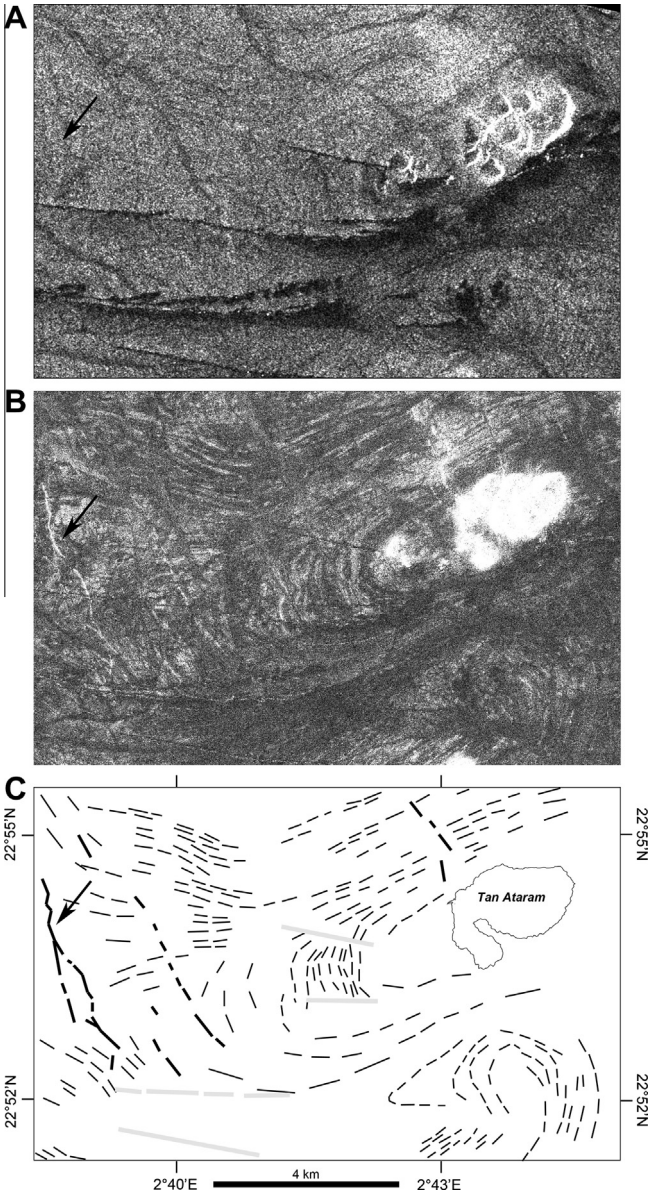

Fig. 6. Comparison of ASAR imagery (C-band) and PALSAR imagery (L-band, FBS mode) on the Tan Ataram area. (A) ASAR, (B) PALSAR, (C) geological sketch with foliation trajectories (thin black lines), dykes (thick black lines), and main dunes (thick gray lines).

Please cite this article in press as: Deroin, J.-P., et al. Integrating geologic and satellite radar data for mapping dome-and-basin patterns in the In Ouzzal Terrane, Western Hoggar, Algeria. J. Afr. Earth Sci. (2014), http://dx.doi.org/10.1016/j.jafrearsci.2014.03.015

Earth's oceans and land with a suite of instruments, one of which was the Advanced Synthetic Aperture Radar (ASAR). The SAR operated in C-band (λ = 5.6 cm), with an off-nadir angle of 23°. Only the VV polarization was available. The pixel size is 12.5 m corresponding to a spatial resolution of 25 m.

4.2.3. Thematic Mapper

The Landsat system is the longest running programme for acquisition of imagery of Earth from space. The Thematic Mapper (TM) is a sensor carried on board Landsat 4- and Landsat 5 satellite launched in 1982 and 1984, respectively. The approximate scene size is 170 km north–south by 183 km east–west. Landsat TM image data consist of seven spectral bands in the visible to the thermal range. We used Landsat data acquired on 3rd March 1987 for identifying the major geological units (Fig. 3).

4.3. Surface roughness and geology

The region under study has arid climate, meaning no soil moisture and consequently no effects of the dielectric constant on backscattering. Test sites used for the present study are located in the In Ouzzal Terrane. It consists of flat morphologies locally invaded by sand blown from the Sahara Desert. The different surfaces comprise (i) contiguous centimetre-size rock fragments (pebbles) forming a relatively flat surface, (ii) scattered pebbles forming a surface of medium roughness, and (iii) oversize pebbles forming a very rough surface. Other surfaces correspond to waterborne deposits or sandy eolian deposits. We determined the nature of the land surface by quantifying and qualifying parameters, such as the maximum and mean heights, and the root-mean-square (rms) height of the rough spots and the lithological nature of each site, using at least one measure per m^2 to define the maximum height and ten measures per m^2 to calculate the mean and rms heights. Basically, the roughness of the 'reg' is related, on the one hand, to the lithological nature of the rocks, i.e. charnockite, metasediment, volcanites, BIF, marbles, etc., and on the other hand, to the geomorphological setting, i.e. substrate, piedmont glacis, structural slope, wadis, etc. (see also Fig. 3). Vertical and oblique photographs of the ground were taken, in order to identify different parameters including the standard deviation of height and the correlation length. Small effects of the profile length on the backscattering coefficients at the medium range of incidence angle have been verified by measurement of natural soil surface (Oh and Hong, 2007). Only manual measurements using rulers and measuring tapes were conducted and no laser profiler was used. A discussion of the method of profile production is given in Mattia et al. (2003). Each test site should cover at least one hectare, i.e. 256 PALSAR pixels. The sigma naught is derived from at least 100 pixels of the radar scenes. The positioning was carried out by using a hand-held Global Positioning System (GPS) receiver. Digital elevation models were used to check the horizontality of the surfaces over large distance. Obvious contrasts in the field

Fig. 7. The ScanSAR data processed with a Gaussian filtering.

Please cite this article in press as: Deroin, J.-P., et al. Integrating geologic and satellite radar data for mapping dome-and-basin patterns in the In Ouzzal Terrane, Western Hoggar, Algeria. J. Afr. Earth Sci. (2014), http://dx.doi.org/10.1016/j.jafrearsci.2014.03.015

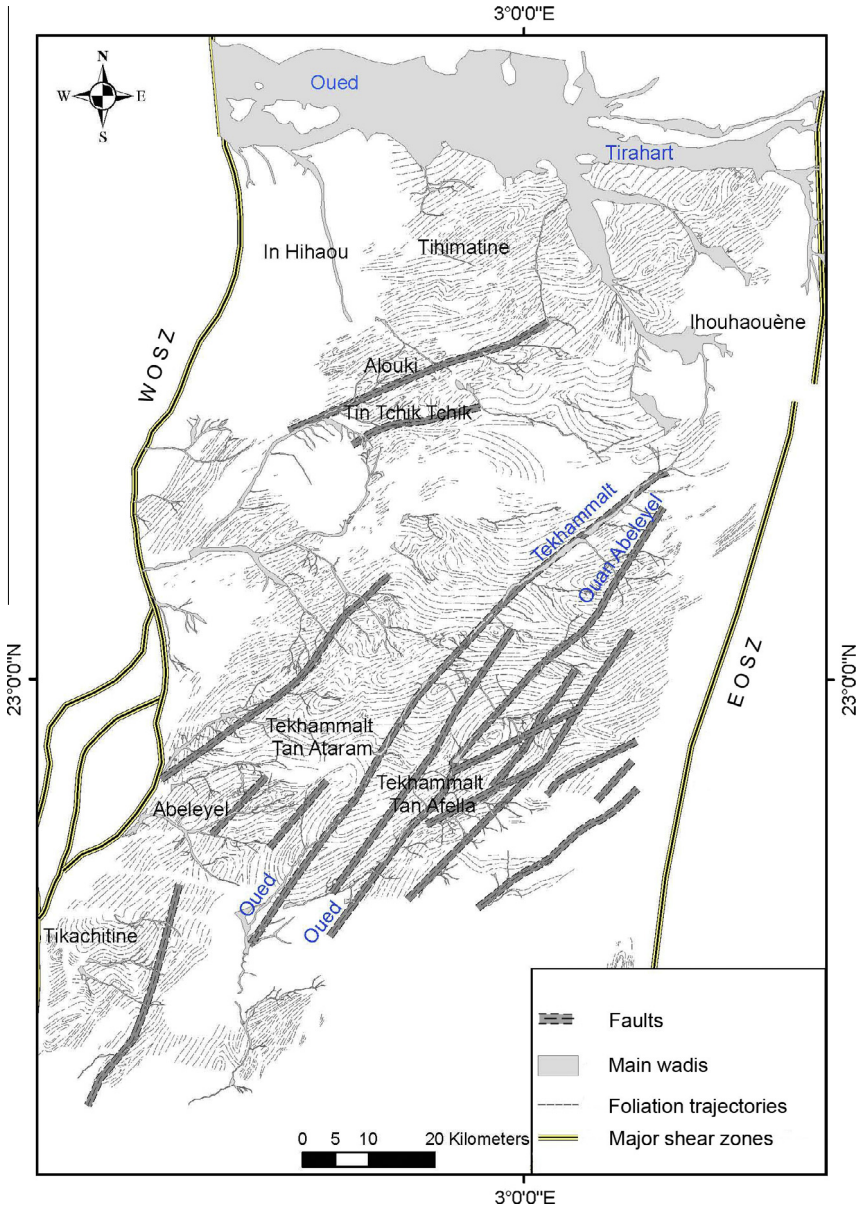

Fig. 8. Interpretation of the ScanSAR data between the West Ouzzalian Shear Zone (WOSZ) and the East Ouzzalian Shear Zone (EOSZ).

(for example when banded iron formation or dykes are concerned) have been used to check the accuracy of the positioning. Horizontal positioning is estimated at 5–10 m and corresponds to less than 2 PALSAR pixels. The Saharan context is particularly favorable to obtain a disperse set of satellites improving the accuracy of the GPS.

5. Results

5.1. Comparison of the L- and C-bands

In Section 1, radar has been shown as particularly relevant in arid region when compared to optical data (Fig. 1). We now briefly evaluate the potential for geological mapping of the C-band of ASAR and the L-band of PALSAR, respectively. Fig. 6 illustrates one of the key points of the In Ouzzal Terrane in the Tan Ataram area. The L-band of PALSAR is clearly more accurate for determining the main foliation trajectories. This pattern allows drawing large-scale folds. Some Proterozoic dykes, mainly NNW–SSE oriented, can be recognized, whereas they are totally unseen on the C-band. It should be mentioned that if the larger wavelength is more favorable to the distinction of the roughness, and thus the lithology, the incident angle is also more interesting with PALSAR (about 34°) than with ASAR (about 23°). This is the reason why the Tan Ataram massif suffers the lay-over phenomenon in the ASAR image. Reliefs are deformed and present a typical V-shape with the point of the V indicating the EW-oriented beam. The pixel size also plays an important role: 6.25 m with PALSAR and 12.5 m with ASAR. The narrow ridges corresponding to the dykes are clear. Outstanding objects may cause preferential backscattering from their edges and corners. This is known as edge effect and corner reflectors (Abdelsalam et al., 2000). This allows SAR to image dykes despite some of them are narrower than the spatial resolution. Orientation of the dykes corresponds approximately to that of the ascending orbit of the PALSAR acquisition. Therefore, the side-looking signal is perpendicular to the

Please cite this article in press as: Deroin, J.-P., et al. Integrating geologic and satellite radar data for mapping dome-and-basin patterns in the In Ouzzal Terrane, Western Hoggar, Algeria. J. Afr. Earth Sci. (2014), http://dx.doi.org/10.1016/j.jafrearsci.2014.03.015

structure, a particularly favorable condition for detecting outstanding objects.

5.2. Large scale mapping using the wide swath mode (ScanSAR)

Interpretation of the ScanSAR image (Fig. 7) put into light some structural features such as the foliation trajectories, ductile faults, large shear zones and corridors, rolling structures, lenses, and sigmoids related to the multiphase tectonics. Most of these features are difficult to distinguish in the field and on remote sensing optical data as well.

The foliation trajectories (Fig. 8) are mainly NE–SW oriented. Two major structural events interfere: on the one hand, the dome-and-basin structures of the northern In Ouzzal Terrane already suggested by Haddoum et al. (1994) and on the other hand, reorientation in the shear zones including the major West- and East-Ouzzalian Shear Zones. Circular, sigmoid or ovoid structures have been generated and large complex folds as well. The field measurements indicate that the foliation is steeply dipping and frequently vertical, except to the south near Tikachitine where the dip is only 50–75°.

Shear zones are revealed by the typical aspect of the foliation which is aligned on tens of kilometers and frequently followed by the main wadis (for instance Oued Tekhamalt and Oued Ouan Abeleyel). Laminated quartzites (mylonites) crop out along these shear zones. Most of the NE–SW shear zones are characterized by sinistral movement, whereas the ENE-WSW shear zones show dextral strike-slip faulting. Bouzid et al. (2008) identified the shear zone corresponding to Oued Ouan Abeleyel within a thickness of 20 km, as it causes a significant fall of resistivity.

A large rolling structure about 20 km long (E–W) and 12 km width (N–S) is shown in the northern part of Oued Tekhamalt, about 20 km to the north of Tan Ataram (Fig. 9). The quartzite layers suffer pinch-and-swell structures, particularly in their southern part. Following Haddoum et al. (1994) we consider this structure as the evidence of former domes that were first folded and subsequently affected by the NE–SW shear zones. Large synforms with a NE–SW axis are recognized, for example near Alouki (Fig. 8).

Field work allows attributing a basic nature to the rocks constituting lenses and a charnockitic origin to the ones forming sigmoids. The main sigmoid is close to Tan Afella (Fig. 9) and is about 25 km long from SW to NE. It is clearly related to the dextral ENE–WSW shear zones previously mentioned.

A later deformation is also recognized owing to the ScanSAR data. Some E–W or N–S faults have been mapped (not shown in Figs. 8 and 9), some of them affecting the East-Ouzzalian Shear Zone. These faults are probably Cretaceous in age.

From a quantitative viewpoint based on intensity of backscatter radar signal (in dB), the smoother areas are the Cretaceous transgression in the southern part of the image (−26.1 dB) and Oued Tirahart (−24.2 dB). These zones appear dark in the image. The Archaean and Palaeoproterozoic In Ouzzal Terrane presents values ranging from −21 to −23 dB. The other areas correspond to mountains and reliefs and the elevated sigma-naught of these landscape-units (white in the image) does not result from a simple scattering but from complex volume, double-bounce, and edge effects. These

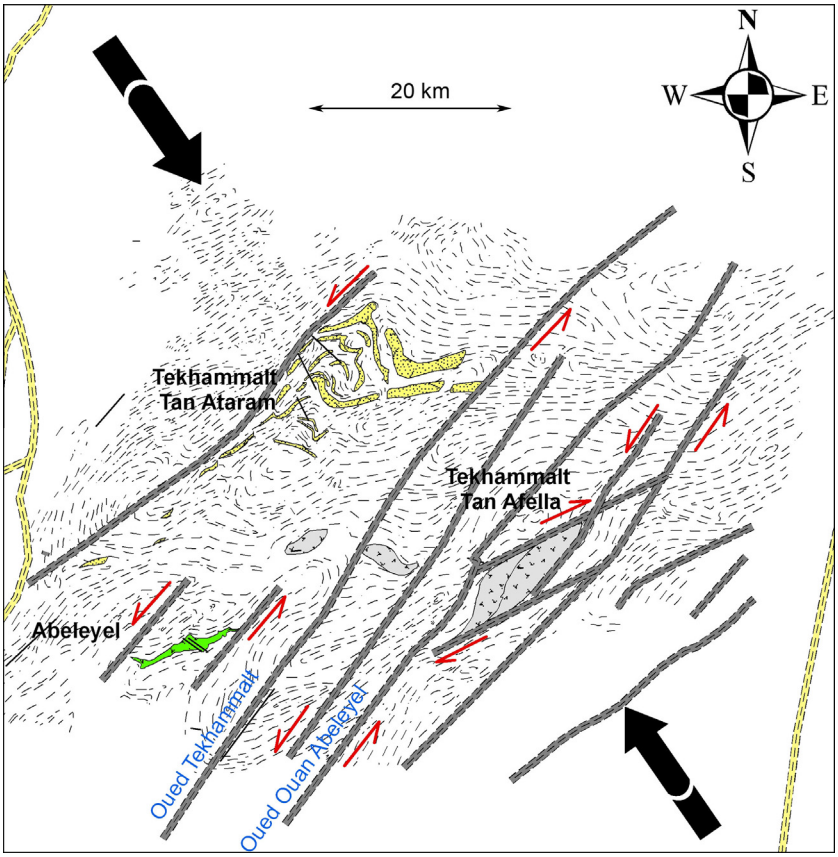

Fig. 9. Focus on the Tekhamalt structures. Green: greenstone basin; Gray: lenses (basic rocks of the basin) and sigmoids (charnockites); Yellow: Quartzites; Black arrows: direction of the compression. Red arrows: sinistral or dextral movement along the fault. See also caption of Fig. 8. (For interpretation of the references to color in this figure legend, the reader is referred to the web version of this article.)

Please cite this article in press as: Deroin, J.-P., et al. Integrating geologic and satellite radar data for mapping dome-and-basin patterns in the In Ouzzal Terrane, Western Hoggar, Algeria. J. Afr. Earth Sci. (2014), http://dx.doi.org/10.1016/j.jafrearsci.2014.03.015

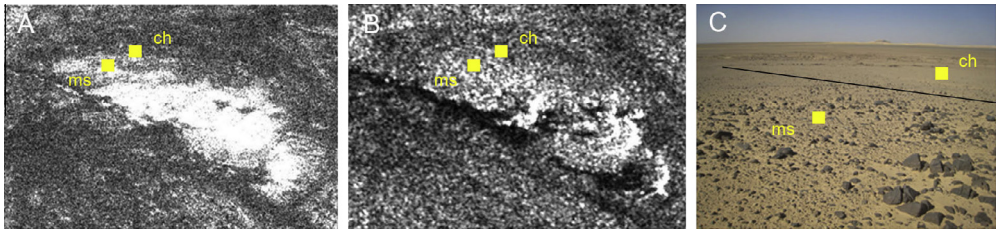

Fig. 10. The Khanfous massif. (A) Palsar FBS. (B) ASAR. (C) Field photograph showing the metasediment (ms) in the foreground and the charnockites (ch) in the background.

results cannot be compared to the results obtained over flat surfaces corresponding to direct backscattering.

5.3. Roughness study: example of the Khanfous

In order to quantify the results in terms of backscattering (with the Fine Beam Single mode of PALSAR), the next step involves analyzing an area where the lithological contrast is marked. The selected place is the so called Khanfous (beetle) massif (Fig. 10). Here, the limit between charnockite and basin formations is clear. The small basin is made primarily of Archaean Al–Mg metasediments with rare basalts. The contrast is particularly obvious in the field (Fig. 10, C). The metasediments are vertically layered with a maximum elevation of about 30 cm high. The charnockites show smaller boulders (maximum elevation above sand surface at about 5 cm) and the outcrops do not allow measuring structural directions. The radiometric calibration gives values ranging from −20.1 dB for the Al–Mg metasediments (ms) to −24.7 dB for the charnockites (ch). Fig. 10A and B show that the limit between metasediments (ms) and charnockite (ch) is better expressed in the PALSAR image (10A) than in the ASAR image (10B). This is mainly due to the interest of the largest wavelength (L-band) already emphasized in Fig. 6.

5.4. Roughness study: example of Tekhamalt-Abeleyel basin

Test sites have been visited in the field of Tekhamalt-Abeleyel Basin, in the heart of the In Ouzzal Terrane. Fig. 11 illustrates the area with the Landsat TM color composite (A) and the PALSAR FBS image (B). Test sites 1 and 2 are isolated in the eastern part of the area and correspond to smooth surfaces (Fig. 12, A and B). Test sites 3 to 6 form a N–S cross section about 1 km long. Note that the structure is also clear in the optical image and characterized by a blue color corresponding to the basin formations spectral signatures.

Note that the area located to the west of test site 1 presents many white stripes in the PALSAR image corresponding to hard rock layers. Fieldwork indicates a small cover above the bedrock, generally less than 30 cm thick, made of mixed sand and gravels, typical of the serir. Serir surfaces provide a homogeneous color in the optical image. In this case the radar signal probably penetrates the dry cover and is backscattered when it meets the hidden rocks. This phenomenon illustrates the volume-scattering and is no more comparable to the direct backscattering of the rough surfaces we investigate in the present study.

The sigma-naught of each selected region of the Tekhamalt-Abeleyel area is given in Table 3, as well as the mean, standard deviation and ratio (mean/standard deviation) for the corresponding digital numbers. The calculated values for other areas are also reported, including the metasediments and charnockites of the Khanfous (see Section 4.3.). The maximum height of the blocks and the root-mean-square (rms) height estimated from direct field measurement are also reported (see Fig. 12). The maximum height of rocks corresponds to the maximum elevation of rocks or boulders in a given area. It can be the absolute value measured in site when the dispersion of values is large (high standard deviation), or an average of many rocks of similar elevation. The value of this parameter is between 0.5 and 30 cm. Statistical parameters such as the standard deviation or correlation length are frequently used to describe roughness quantitatively. Here, we use the root-mean-square height, the value of which is between 0.05 and 2.10 cm.

Results indicate a good correlation between backscattering expressed by the calibrated sigma-naught and the maximum height and the rms height, respectively (Fig. 13). The best relationship between the sigma-naught and the maximum height seems to be a logarithmical relation with a correlation of 91% ($R^2 = 0.82$). The best relationship between the sigma-naught and the rms height seems to be a linear relation with the same correlation.

6. Discussion-conclusion

6.1. Roughness parameter and rocks of the IOT

Most of desert rough surfaces of the In Ouzzal Terrane show a sigma-naught comprised between – 20 dB for a very rough surface and – 26 dB for a very smooth surface. The lower noise level detectable on the PALSAR image is estimated at about – 34 dB (Shimada et al., 2009). Note that when the surface is no more horizontal but corresponds to a massif or a mountain, outstanding objects cause preferential backscattering from their edges and

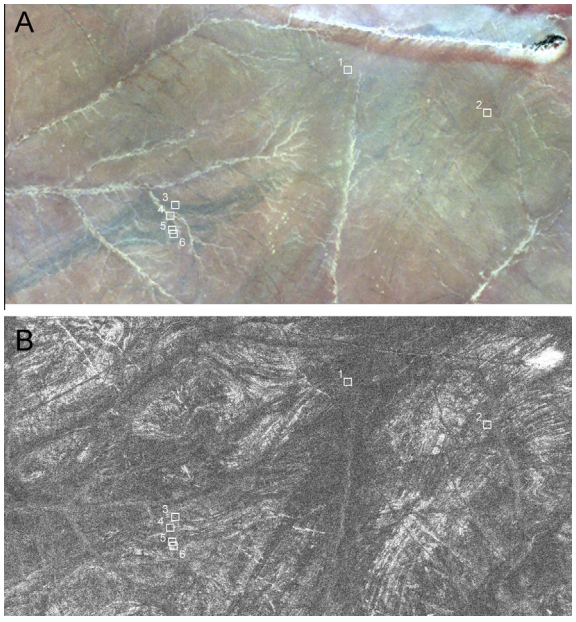

Fig. 11. Basin of Abeleyel. Comparison of the optical Landsat TM and radar ALOS PALSAR. Sites 1 to 6 correspond to photographs A to F (Fig. 12).

Please cite this article in press as: Deroin, J.-P., et al. Integrating geologic and satellite radar data for mapping dome-and-basin patterns in the In Ouzzal Terrane, Western Hoggar, Algeria. J. Afr. Earth Sci. (2014), http://dx.doi.org/10.1016/j.jafrearsci.2014.03.015

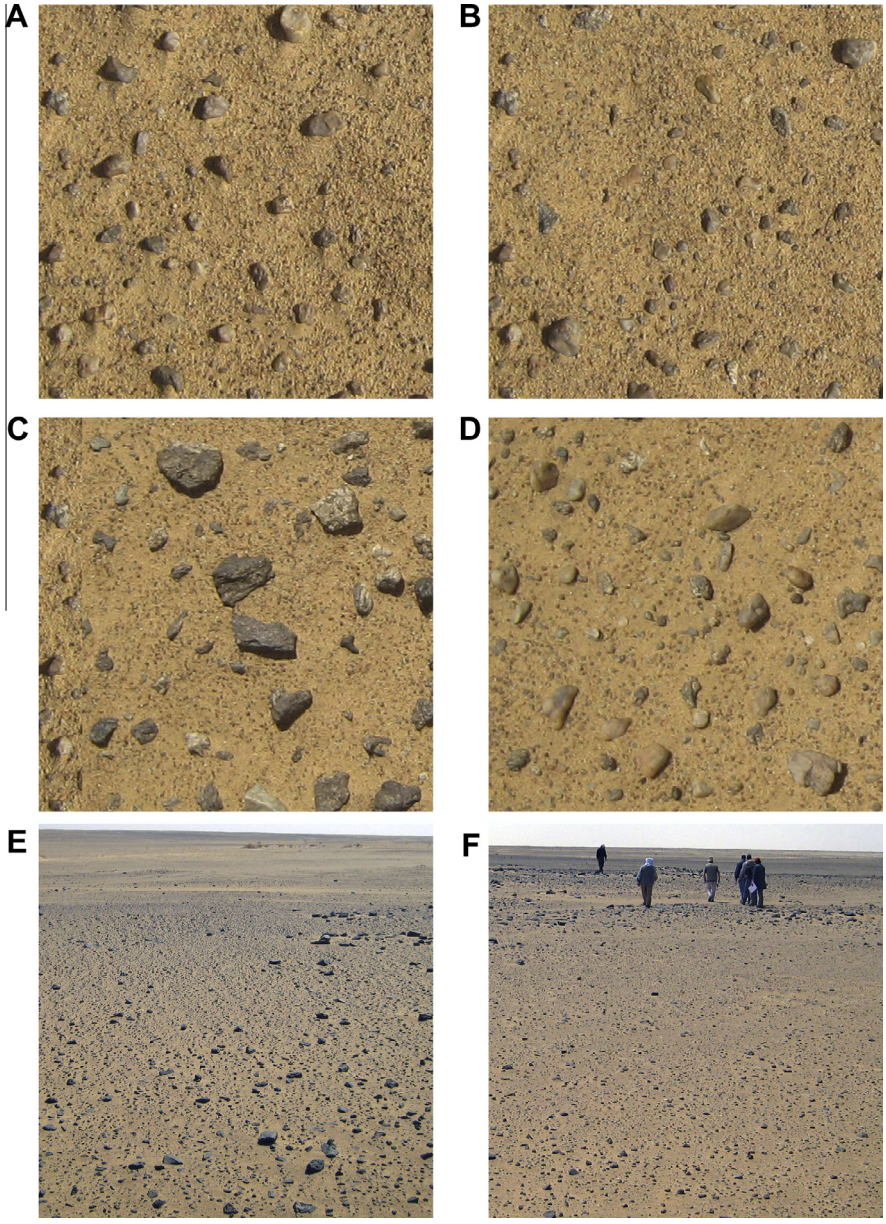

Fig. 12. Basin of Abeleyel. (A and B) Typical smooth surfaces ((A) on basin formations, (B) on charnockites). (C and D) Typical medium rough surfaces ((C) on quartzites with clinopyroxene, (D) on unidentified basin formation). (E and F) Oblique view of landscapes showing rough surface due to gneiss with garnet and sillimanite (E) or gabbro-norite (F). (A)–(D) correspond to vertical views 20 cm × 20 cm (see also Fig. 4).

corners. Backscattering phenomenon is complicated by volume scattering (double-bounce), edge effects and normal reflection. This is the reason why we only use homogeneous flat surfaces for estimating the backscattering.

A breakpoint between smooth and rough surfaces (and the corresponding dominant radar scattering mechanisms) is loosely implied by the empirical Rayleigh criterion. The Rayleigh criterion $\Re$ modified by Peake and Oliver (1971) provides a good estimate of the range to be considered to interpret the surface roughness influence. Considering λ as the PALSAR wavelength (23.6 cm) and θ, the local incident angle (34.3°), the backscattering ranges between (1) and (3):

(1) smooth surface if rms $\leqslant \lambda/25\cos\theta$, $\Re_{34.3^\circ}$ = 1.14 cm,
(2) intermediate surface if rms = $\lambda/8\cos\theta$, $\Re_{34.3^\circ}$ = 3.57 cm,
(3) rough surface if rms $\geqslant \lambda/4.4\cos\theta$, $\Re_{34.3^\circ}$ = 6.49 cm.

Therefore, the sensitivity of L-band PALSAR data to roughness ranges theoretically from 1 to 6.5 cm. In our case, most places show small rms values and the maximum elevation of height can be used to roughly define smooth, intermediate, and rough surfaces. The smoother places correspond to deflation sands (without ridges) and alluvial deposits ($\leqslant -26$ dB). They appear dark in the image. Their maximum height is less than 0.5 cm. Most of the reg formed on charnockites, quartzites, and gabbro-pyroxenites present values between −23 and −25.5 dB (maximum height between 0.5 and 4 cm). The ratio mean/standard deviation (DN) is in the range 4–7, characterizing relatively homogeneous areas. Rougher reg formed on Al–Mg metasediments, alkaline granite, banded iron formations, and quartz-rich rocks present values between −20 and −23 dB (maximum height between 2 and 7 cm), with the ratio mean/standard deviation (DN) in the range 2–5 (the surfaces are relatively heterogeneous). These three categories

Please cite this article in press as: Deroin, J.-P., et al. Integrating geologic and satellite radar data for mapping dome-and-basin patterns in the In Ouzzal Terrane, Western Hoggar, Algeria. J. Afr. Earth Sci. (2014), http://dx.doi.org/10.1016/j.jafrearsci.2014.03.015

Table 3
Calculated DN value and sigma-naught for test sites of Tekhamalt-Abeleyel Basin and other areas. Maximum elevation and rms height are also added.

	DN (mean)	DN (std d)	Mean/std d	Sigma naught (dB)	Maximum elevation	Rms height
Tekhamalt-Abeleyel (Fig. 11)						
1. Charnockite	818.67	±224.59	3.65	−25.2	2 cm	0.15 cm
2. Reg on basin fms	703.11	±313.49	2.24	−26.5	1.5 cm	0.10 cm
3. Qzte with gnt and sill	1120.89	±211.84	5.29	−22.4	7 cm	1.30 cm
4. Qzte with opx	838.11	±134.58	6.23	−24.9	3 cm	0.65 cm
5. Gneiss with gnt and sill	859.33	±100.18	8.58	−24.7	3.5 cm	0.95 cm
6. Gabbro-norite	934.67	±186.67	5.01	−24.2	3 cm	0.85 cm
Khanfous (Figure 10)						
7. Metasediments Khanfous	1466.33	±429.72	3.41	−20.1	30 cm	2.10 cm
8. Charnockites Khanfous	917.83	±134.72	6.81	−24.7	4 cm	0.55 cm
Other areas						
9. Reg with quartz boulders (1)	1009.55	±417.10	2.42	−23.3	3 cm	1.05 cm
10. Banded Iron Formation	1110.00	±298.10	3.72	−22.5	2 cm	0.80 cm
11. Charnockites	988.66	±205.92	4.80	−23.5	1 cm	0.05 cm
12. Reg with quartz boulders (2)	1199.94	±376.09	3.19	−21.8	5 cm	1.40 cm
13. Reg on basin fms	751.21	±128.67	5.84	−25.9	0.5 cm	0.05 cm
14. Qzte with opx	838.21	±118.92	7.05	−24.9	2 cm	0.08 cm

Abbreviations: fms: formations, gnt: garnet, opx: orthopyroxene, qzte: quartzite; sill: sillimanite.

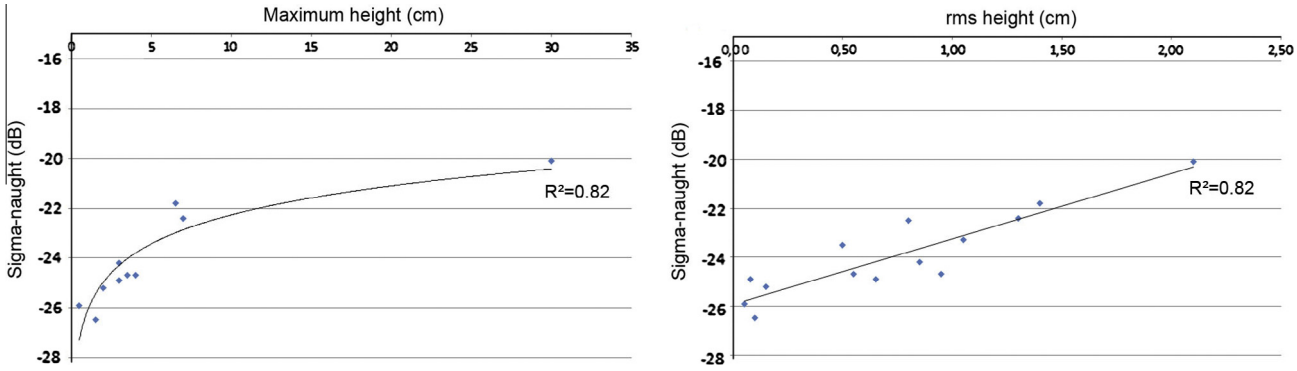

Fig. 13. Relation between the calculated PALSAR FBS sigma-naught in dB and the maximum height of the blocks (left plot) and the root-mean-square (rms) height (right plot).

correspond to direct backscattering of more or less rough surfaces. Higher sigma-naught are given by very rough surfaces associated with outstanding reliefs such as dolerite dykes or massive quartzite (−13 to −14 dB).

The smoothest reg surface is composed of small juxtaposed rock fragments (average height close to 0.5 cm) forming a pebble 'micro-pavement' at the surface. The roughest reg surface contains larger pebbles (average height close to 5 cm). The surfaces of intermediate roughness show that pebble size and distinction against the sandy matrix increase with increasing roughness and greater rms height.

6.2. The dome-and-basin pattern in the In Ouzzal Terrane

Archaean cratons are amongst the principal reservoirs of Earth's mineral resources. Archaean geodynamics is a debate of great interest, particularly as it concerns the formation, differentiation and reworking of continents (Nisbet and Fowler, 1983; Peschler et al., 2004; Cagnard et al., 2011; Harris et al., 2012). The principal question is whether large-scale vertical displacements were predominant tectonic processes, or the Archaean continents were accreted and reworked by successive collisions at subduction zones as in the present-day plate tectonic paradigm (Peschler et al., 2004). In Early Archaean greenstone terranes, the typical dome-and-basin structure has been cited as evidence of a major tectono-magmatic process, the so called crustal diapirism (Choukroune et al., 1995, 1997; Bouhallier et al., 1995). In this sketch, batholiths composed of tonalite–trondhjemite–granodiorite (TTG) gneisses form the cores of broad structural domes, which are surrounded by narrow synformal belts of greenstone (ultramafic and mafic volcanics) and overlying sedimentary rocks. The dome-and-basin structures are attributed to diapirism, rather than to regional fold interference patterns, because the domes and basins affect rocks of both high and low metamorphic grades as in the Kaapval craton, South Africa, the Dharwar craton, India, and in the Pilbara terrane, Australia. Geophysical models were proposed to further explain dome-and-basin structures and batholith emplacement. Starting from the dichotomy in batholith shapes at depth Peschler et al. (2004) indicate a change, during Late Archaean time, in the processes leading to batholith formation. The post-2.8 batholiths would be akin to the tabular shapes known to be most typical of large plutonic complexes emplaced in many Phanerozoic belts. Other models have been proposed such as the 'dome-and-syncline' or 'dome-and-keel' structure.

The dome-and-basin architectural structure has been applied to the In Ouzzal Terrane (Haddoum et al., 1994; Ouzegane et al., 2003b). Djemai (2008) demonstrated that some lithologies, particularly those of the greenstone belts, can be distinguished using Landsat imagery. In the present study, the PALSAR sensor has been shown to be of great interest, either with high resolution mode (FBS) or large-scale mode (ScanSAR), especially for identifying the foliation trajectories and discriminating the hard-rock layers. The foliation trajectories outline dome-and-basin structures in which supracrustal rocks of greenstone belts occupy the basins. The foliation trajectories are perturbed only by bands of later transcurrent shearing. Variations in structural directions depend on the geometry of plutonic bodies within which the foliation has a domal form. Changes in the intensity of deformation are

essentially limited to boundaries between granitoids and supracrustal series. Remote sensing is then highly complementary to field work, whereas large-scale geophysical survey such as magnetotelluric prospection does not allow separating dome and basin structures (Bouzid et al., 2008).

7. Conclusions

The ALOS spacecraft system with its radar sensor (PALSAR) is particularly relevant for studying arid areas such as the In Ouzzal region. The characterization of most of the landscape units is possible, including mineral surfaces. The dome-and-basin structure is clearly evidenced, whereas it was only suggested. The quantitative approach indicates a good correlation between backscattering and surface roughness parameters. The In Ouzzal Terrane is particularly adapted to the study, because the area is flat, with rare outcrops, and its remoteness hampers field missions to be easily carried out. Therefore, the potential for synthetical geological mapping is large.

The most significant advantages of the synthetic aperture radar (SAR) in geologic studies are the sensitivity to surface parameters and the ability to penetrate dry sand and collect images of shallow sub-surface features. When compared to the C-band of ENVISAT ASAR, ALOS PALSAR perfectly illustrates the fact that longer wavelength results in deeper radar penetration. More generally, ALOS PALSAR illustrates the great potential of the SAR for mapping different rock weathering types differently and then producing different roughness levels, although SAR is generally considered less useful for lithological mapping than orbital visible and infrared images.

Roughness is described by the autocorrelation function and the standard deviation of the roughness height (rms). Thus, the rms height relative to wavelength can be estimated from the inversion of theoretical model. In the future, we envisage calculating these parameters using the principle proposed by Fung et al. (1992) and Shi et al. (1997), and developed by Gade et al. (2008) and Deroin (2012) in the specific case of tidal flats. The method is based on the use of a set of radar data acquired in two different bands (for example C-band and L-band) and allows extracting the field parameters, particularly the rms height. Arid test sites can help prevent moisture and salinity issues typical of the tidal-flat areas. Note that field observation is necessary to properly decipher the relation between backscattering and geophysical parameters.

A launch of ALOS 2 is scheduled for 2014. It will open up new perspectives because it will provide a new class of high quality L-band SAR products. ALOS 2 will have a spotlight mode (1–3 m) and a high resolution mode (3–10 m), whilst PALSAR FBS has a 6.25 m resolution (Kankaku et al., 2009). Fortunately, the wide swath mode of ScanSAR is also planned on board ALOS 2, the resolution and swath being almost equal to PALSAR.

Acknowledgements

The present research was conducted under the PICS project ‘Architecture lithosphérique et dynamique du manteau sous le Hoggar (CNRS-IPG, France, USTHB, Algeria)’. The ALOS data were obtained under the ADEN ALOS agreement No. 3643 ‘Geological mapping of Sensitive Environment’ supported by the Japanese Exploration and Aerospace Agency (JAXA) and the European Space Agency (ESA). The authors would like particularly to thank Dr Masanobu Shimada (JAXA, Japan) and Pr Éric Pottier (University of Rennes, France) for information and feedback on the PALSAR images. The LANDSAT data were downloaded from the USGS website (http://edcsns17.cr.usgs.gov/EarthExplorer/). We are particularly indebted to the Algerian army and OPNA (Office du Parc National de l’Ahaggar) for assistance with field work in the remote In Ouzzal area.

References

Abdelsalam, M.G., Robinson, C., El-Baz, F., Stern, R.J., 2000. Applications of orbital imaging radar for geologic studies in arid regions: the Saharan testimony. Photogramm. Eng. Remote Sens. 66, 717–726.

Ait-Djafer, S., Ouzegane, K., Liégeois, J.P., Kienast, J.R., 2003. Petrology and geochemistry of archean anorthositic complexes from the In Ouzzal granulitic terrane (NW Hoggar, Algeria). J. Afr. Earth Sci. 37, 313–330.

Allègre, C., Caby, R., 1972. Chronologie absolue du Précambrien de l’Ahaggar occidental. Comptes Rendus de l’Académie des Sciences de Paris 275, 2095–2098.

Archer, D.J., Wadge, G., 2001. Modeling the backscatter response due to salt crust development. IEEE Trans. Geosci. Remote Sens. 39, 2307–2310.

Ben Othman, D., Polvé, M., Allègre, C.J., 1984. Nd-Sr isotopic composition of granulites and constraints on the evolution of the lower continental crust. Nature 307, 510–515.

Bernard-Griffiths, J., Fourcade, S., Kienast, J.R., Peucat, J.J., Martineau, F., Rahmani, A., 1996. Geochemistry and isotope Sr, Nd, O study of Al–Mg granulites from the In Ouzzal Archaean block Hoggar, Algeria. J. Metamorph. Geol. 14, 709–724.

Black, R., Latouche, L., Liégeois, J.P., Caby, R., Bertrand, J.M., 1994. Pan-African displaced terranes in the Tuareg shield (central Sahara). Geology 22, 641–644.

Bouhallier, H., Chardon, D., Choukroune, P., 1995. Strains patterns in Archaean domes-and-basin structures: The Dharwar craton Karnataka, South India. Earth Planet. Sci. Lett. 135, 57–76.

Bouzid, A., Akacem, N., Hamoudi, M., Ouzegane, K., Abtout, A., Kienast, J.R., 2008. Magnetotelluric modeling of the deep geologic structure of In Ouzzal Granulitic Unit (western Hoggar). C.R. Geosci. 340, 711–722.

Brahmi, B., Djemai, S., Bendaoud, A., Haddoum, H., Berraki, F., Deroin, J.-P., Kienast, J.-R., Ouzegane, K., 2012. Utilisation des images Landsat 7 ETM+ et ALOS Scansar pour la cartographie de la déformation contemporaine du métamorphisme paléoprotérozoïque de très haute température de l’In Ouzzal Nord (Hoggar, Algérie). Photo-Interprétation Eur. J. Appl. Remote Sens. 48, 18–25, 18–25 and 50–59.

Caby, R., 1970. La chaîne Pharusienne dans le NW de l’Ahaggar Central Sagara. Publication des Mines et de la Géologie, Alger, 289p.

Caby, R., 1996. A review of the In Ouzzal granulitic terrane, Tuareg shield, Algeria: its significance within the Pan-African Trans-Saharan Belt. J. Metamorph. Geol. 14, 659–666.

Caby, R., 2003. Terrane assembly and geodynamic evolution of central–western Hoggar: a synthesis. J. Afr. Earth Sci. 37, 133–159.

Caby, R., Bertrand, J.M., 1977. Synthèse des connaissances sur la géologie du Hoggar. In: «Inventaire et prospective des ressources minérales au Hoggar», Société Nationale de Recherches et d’Exploitation Minières (SONAREM), 293pp.

Cagnard, F., Barbey, P., Gapais, D., 2011. Transition between “Archaean-type” and “modern-type” tectonics: insights from the Finnish Lapland Granulite Belt. Precambr. Res. 187, 127–142.

Chaussard, E., Amelung, F., Abidin, H., Hong, S.H., 2013. Sinking cities in Indonesia: ALOS PALSAR detects rapid subsidence due to groundwater and gas extraction. Remote Sens. Environ. 128, 150–161.

Chernicoff, C.J., Nash, C.R., 2002. Geological interpretation of Landsat TM imagery and aeromagnetic survey data, northern Precordillera region, Argentina. J. S. Am. Earth Sci. 14, 813–820.

Chorowicz, J., Dhont, D., Collet, B., Lichtenegger, J., Barbieri, M., 2005. Spaceborne Radar Applications in Geology. An Introduction to Imaging Radar, and Application Examples of ERS SAR in Geology and Geomorphology, vol. TM-17. ESA Publications Division, ESTEC, Noordwijk, The Netherland, 230p.

Choukroune, P., Bouhallier, H., Arndt, N.T., 1995. Soft lithosphere during periods of Archaean crustal growth or crustal reworking. Geol. Soc. Spec. Publ. 95, 67–86.

Choukroune, P., Ludden, J.N., Chardon, D., Calvert, A.J., Bouhallier, H., 1997. Archaean growth and tectonic processes: a comparaison of the Superior province, Canada and the Dharwar Craton, India. Geol. Soc. Spec. Pub. 121, 63–98.

Daniels, J., Blumberg, D.G., Vulfson, L.D., Kotlyar, A.L., Freiliker, V., Ronen, G., Ben-Asher, J., 2003. Microwave remote sensing of physically buried objects in the Negev Desert: implications for environmental research. Remote Sens. Environ. 86, 243–256.

Denaeyer, M.E., 1934. Matériaux pour l’étude chimico-minéralogique des roches éruptives du Sahara central et soudanais. Bulletin de la Société Française de Minéralogie 57, 284–337.

Deroin, J.P., 2012. Combining ALOS and ERS-2 SAR data for characterization of tidal flats. Case study from the Baie des Veys, Normandy, France. Int. J. Appl. Earth Obs. Geoinf. 18, 183–194.

Deroin, J.P., Delor, C., 2010. Remote sensing and geophysical investigations in French Guiana. Zeitschrift für Geomorphologie 54, 511–534.

Deroin, J.-P., Rudant, J.-P., Wadsworth, A., 1991. Apport du radar imageur SAR au suivi de structures géologiques à terre et en mer. Exemple de l’île de Wight (Manche centrale). Comptes Rendus de l’Académie des Sciences de Paris 312, 1099–1106.

Deroin, J.P., Company, A., Simonin, A., 1997. An empirical model for interpreting the relationship between backscattering and arid land surface roughness as seen with the SAR. IEEE Trans. Geosci. 35 (1), 86–91.

Please cite this article in press as: Deroin, J.-P., et al. Integrating geologic and satellite radar data for mapping dome-and-basin patterns in the In Ouzzal Terrane, Western Hoggar, Algeria. J. Afr. Earth Sci. (2014), http://dx.doi.org/10.1016/j.jafrearsci.2014.03.015

Deroin, J.P., Motti, E., Simonin, A., 1998. Comparison of potential for using optical data and synthetic aperture radar for geological mapping in arid regions (Atar, Western Sahara, Mauritania). Int. J. Remote Sens. 19 (6), 1115–1132.

Desnos, Y.-L., Buck, C., Guijarro, J., Levrini, G., Suchail, J.-L., Torres, R., Laur, H., Closa, J., Rosich, B., 2000. The ENVISAT advanced synthetic aperture radar system. In: Proceedings of International Geoscience and Remote Sensing Symposium, IGARSS'00 3, pp. 1171–1173.

Djemai, S., 1996. Les pyrigarnites et les granulites alumineuses d'Amesmessa, Môle In Ouzzal, Hoggar: Relations de phases et déformation. Magister USTHB, Algiers, 210pp. (unpublished).

Djemai, S., 2008. Etude structurale et pétrologique des séries précambriennes de la terminaison sud de l'unité granulitique de l'In Ouzzal (Hoggar occidental). Doctorate of Science, USTHB, Algiers, 200pp. (unpublished).

Elachi, C., Granger, J., 1982. Spaceborne imaging radars probe 'in depth'. IEEE Spectr. 19, 24–29.

Elachi, C., Cimino, J.B., Granger, J., 1985. Remote sensing of the Earth with spaceborne imaging radars. Prog. Astronaut. Aeronaut. 97, 639–683.

Evans, D.L., Farr, T.G., Van Zyl, J.J., 1992. Estimates of surface roughness derived from synthetic aperture radar (SAR) data. IEEE Trans. Geosci. Remote Sens. 30, 382–389.

Evans, D.L., Plaut, J.J., Stofan, E.R., 1997. Overview of the Spaceborne Imaging Radar-C/X-Band Synthetic Aperture Radar (SIR-C/X-SAR) missions. Remote Sens. Environ. 59, 135–140.

Evans, D.L., Alpers, W., Cazenave, A., Elachi, C., Farr, T., Glackin, D., Holt, B., Jones, L., Liu, W.T., McCandless, W., Menard, Y., Moore, R., Njoku, E., 2005. Seasat – A 25-year legacy of success. Remote Sens. Environ. 94, 384–404.

Ferrara, G., Gravelle, M., 1966. Radiometric ages from western Ahaggar (Sahara) suggesting an eastern limit for, the west African craton. Earth Planet. Sci. Lett. 1, 319–324.

Fung, A.K., Li, Z., Chen, K.S., 1992. Backscattering from a randomly rough dielectric surface. IEEE Trans. Geosci. Remote Sens. 30, 356–369.

Gade, M., Alpers, W., Melsheimer, C., Tanck, G., 2008. Classification of sediments on exposed tidal flats in the German Bight using multi-frequency radar data. Remote Sens. Environ. 112, 1603–1613.

Gani, N.D.S., Abdelsalam, M.G., 2006. Remote sensing analysis of the Gorge of the Nile, Ethiopia with emphasis on Dejen-Gohatsion region. J. Afr. Earth Sci. 44, 135–150.

Ganne, M., Gerbault, M., Block, S., 2014. Thermo-mechanical modeling of lower crust exhumation. Constraints from the metamorphic record of the Palaeoproterozoic Eburnean orogeny, West African Craton. Precambr. Res. 243, 88–109.

Giraud, P., 1961. Les charnockites et les roches associées du Sugarien à faciès In Ouzzal (Sahara algérien). Bulletin de la Société Géologique de France 3, 165–170.

Gravelle, M., 1969. Recherches sur la géologie du socle Précambrien de l'Ahaggar centro-occidental dans la région de Silet Tibehaouine. PhD Thesis, Paris, 781pp. (unpublished).

Guiraud, M., Kienast, J.R., Ouzegane, K., 1996. Corundum–quartz bearing assemblage in the Ihouhaouene area In Ouzzal, Algeria. J. Metamorph. Geol. 14, 755–761.

Haddoum, H., Choukroune, P., Peucat, J.J., 1994. Structural evolution of the Precambrian In Ouzzal massif, Central Sahara, Algeria. Precambr. Res. 65, 155–166.

Hadj-Kaddour, Z., Liégeois, J.P., Demaiffe, D., Caby, R., 1998. The alkaline–peralkaline granitic post-collisional Tin Zebane dyke swarm (Pan-African Tuareg shield, Algeria): prevalent mantle signature and late agpaitic differentiation. Lithos 45, 223–243.

Harris, L.B., Godin, L., Yakymchuk, C., 2012. Regional shortening followed by channel flow induced collapse: a new mechanism for "dome and keel" geometries in Neoarchaean granite-greenstone terrains. Precambr. Res. 212–213, 139–154.

Inzana, J., Kusky, T., Higgs, G., Tucker, R., 2003. Supervised classifications of Landsat TM band ratio images and Landsat TM band ratio image with radar for geological interpretations of central Madagascar. J. Afr. Earth Sci. 37, 59–72.

Kankaku, Y., Osawa, Y., Suzuki, S., Watanabe, T., 2009. The overview of the L-band SAR onboard ALOS-2. In: Progress In Electromagnetics Research Symposium Proceedings, Moscow, pp. 735–738.

Kienast, J.R., Ouzegane, K., 1987. Polymetamorphic Al–Mg rich parageneses in Archean rocks from Hoggar, Algeria. Geol. J. 22, 57–79.

Kienast, J.R., Fourcade, S., Guiraud, M., Hensen, B.J., Ouzegane, K. (Eds.), 1996. Special issue on the In Ouzzal Granulite unit, Hoggar, Algeria. J. Metamor. Geol. 14, 659–808.

Kusky, T.M., Ramadan, M.R., 2002. Structural controls on Neoproterozoic mineralization in the South Eastern Desert, Egypt: an integrated field, Landsat TM, and SIR-C/X SAR approach. J. Afr. Earth Sci. 35, 107–121.

Lancelot, J.R., Vitrac, A., Allègre, C.J., 1976. Uranium and lead isotopic dating with grain-by-grain zircon analysis: a study of a complex geological history with a single rock. Earth Planet. Sci. Lett. 29, 357–366.

Lelubre, M., 1952. Recherches sur la géologie de l'Ahaggar central et occidental (Sahara central). Doctorate of Sciences (doctorat d'Etat), Paris, vol. 1 (354pp), vol. 2 (385pp).

Mattia, F., Davidson, F.W.J., Le Toan, T., D'Haese, C.M.F., Verhoest, N.E.C., Gatti, A.M., Borgeaud, M., 2003. A comparison between soil roughness statistics used in surface scattering models derived from mechanical and laser profilers. IEEE Trans. Geosci. Remote Sens. 41 (7), 1659–1671.

McCauley, J.F., Schaber, G.G., Breed, C.S., Grolier, M.J., Haynes, C.V., Issawi, B., Elachi, C., Blom, R., 1982. Subsurface valleys and geoarchaeology of the Eastern Sahara revealed by Shuttle Radar. Science 218, 1004–1020.

McCauley, J.F., Breed, C.S., Schaber, G.G., McHugh, W.P., Issawi, B., Haynes, C.V., Grolier, M.J., El Kilani, A., 1986. Paleodrainages of the Eastern Sahara – The radar rivers revisited (SIR-A/B Implications for a Mid-Tertiary Trans-African Drainage System). IEEE Trans. Geosci. Remote Sens. 24, 624–648.

Nisbet, E.G., Fowler, C.M.R., 1983. Model for Archean plate tectonics. Geology 11, 376–379.

Oh, Y., Hong, J.Y., 2007. Effects of surface profile length on the backscattering coefficients of bare surfaces. IEEE Trans. Geosci. Remote Sens. 45 (3), 632–638.

Ouzegane, K., 1987. Les granulites Al-Mg et les carbonatites dans la série de l'In Ouzzal NW Hoggar, Algérie. Nature et évolution de la croûte continentale profonde pendant l'Archéen. Doctorate of Sciences, Paris, 433pp.

Ouzegane, K., Guiraud, M., Kienast, J.R., 2003a. Prograde and retrograde evolution in high temperature corundum granulites FMAS and KFMASH systems from In Ouzzal terrane, NW Hoggar, Algeria. J. Petrol. 44, 517–545.

Ouzegane, K., Kienast, J.R., Bendaoud, A., Drareni, A., 2003b. A review of Archaean and Paleoproterozoic evolution of the In Ouzzal granulitic terrane (Western Hoggar, Algeria). J. Afr. Earth Sci. 37, 207–227.

Ouzegane, K., Liégeois, J.P., Kienast, J.R., 2003c. The Precambrian of Hoggar massif, Tuareg Shield. Special Issue J. Afr. Earth Sci. 37, 123–350.

Paillou, P., Grandjean, G., Baghdadi, N., Heggy, E., August-Bernex, T., Achache, J., 2003. Subsurface imaging in south-central Egypt using low-frequency radar: Bir Safsaf revisited. IEEE Trans. Geosci. Remote Sens. 41, 1672–1684.

Pal, S.K., Majumdar, T.J., Bhattacharya, A.K., 2007. ERS-2 SAR and IRS-1C LISS III data fusion: A PCA approach to improve remote sensing based geological interpretation. ISPRS J. Photogramm. Remote Sens. 61, 281–297.

Peake, W.H., Oliver, T.L., 1971. The Response of Terrestrial Surfaces at Microwave Frequencies, Columbus, Ohio: Ohio State University, Electroscience Laboratory, 2440–7, Technical, Report AFAL-TR-70301.

Peschler, A.P., Benn, K., Roest, W.R., 2004. Insights on Archean continental geodynamics from gravity modelling of granite–greenstone terranes. J. Geodyn. 38, 185–207.

Peucat, J.J., Capdevila, R., Drareni, A., Choukroune, P., Fanning, M., Bernard-Griffiths, J., Fourcade, S., 1996. Major and trace element geochemistry and isotope Sr, Nd, Pb, O systematics of an Archaean basement involved in a 2.0 Ga VHT 1000°C metamorphic event. In Ouzzal massif, Hoggar, Algeria. J. Metamorph. Geol. 14, 667–692.

Raharimahefa, T., Kusky, T.M., 2006. Structural and remote sensing studies of the southern Betsimisaraka Suture, Madagascar. Gondwana Res. 10, 186–197.

Reboul, C., Moussu, H., Lessard, L., 1962. Notice explicative de la carte géologique au 1/500 000 du Hoggar (Sahara central). Bureau de Recherches Géologiques et Minières, 104pp.

Rémond, A., Deroin, J.P., 1997. Empirical and theoretical backscattering behavior as a function of roughness for arid land surfaces. In: Proceedings of International Geoscience and Remote Sensing Symposium, IGARSS'97 4, pp. 1612–1614.

Rosenqvist, A., Shimada, M., Ito, N., Watanabe, M., 2007. ALOS PALSAR: a pathfinder mission for global-scale monitoring of the environment. IEEE Trans. Geosci. Remote Sens. 45, 3307–3316.

Rudant, J.P., Deroin, J.P., Polidori, L., 1994. Multi-resolution analysis of radar images and its application to lithological and structural mapping: Larzac (Southern France) test site. Int. J. Remote Sens. 15, 2451–2468.

Schaber, G.G., 1999. SAR studies in the Yuma Desert, Arizona: sand penetration, geology, and the detection of military ordnance debris. Remote Sens. Environ. 67, 320–347.

Schaber, G.G., Breed, C.S., 1999. The importance of SAR wavelength in penetrating blow sand in Northern Arizona. Remote Sens. Environ. 69, 87–104.

Schaber, G.G., McCauley, J.F., Breed, C.S., Olhoeft, G.R., 1986. Shuttle imaging radar: physical controls on signal penetration and subsurface scattering in the Eastern Sahara. IEEE Trans. Geosci. Remote Sens. 24, 603–623.

Schaber, G.G., McCauley, J.F., Breed, C.S., 1997. The use of multifrequency and polarimetric SIR-C/X-SAR data in geologic studies of Bir Safsat, Egypt. Remote Sens. Environ. 59, 337–363.

Shi, J., Wang, J., Hsu, A.Y., O'Neill, P.E., Engman, E., 1997. Estimation of bare surface soil moisture and surface roughness parameters using L-band SAR image data. IEEE Trans. Geosci. Remote Sens. 35, 1254–1266.

Shimada, M., Isogushi, O., Tadono, T., Isono, K., 2009. PALSAR radiometric calibration and geometric calibration. IEEE Trans. Geosci. Remote Sens. 47, 3915–3932.

Singhroy, V.H., 2001. Geological applications of RADARSAT-1: a review. In: Proceedings IGARSS'01 1, pp. 468–470.

Thurmond, A.K., Abdelsalam, M.G., Thurmond, J.B., 2006. Optical-radar-DEM remote sensing data integration for geological mapping in the Afar Depression, Ethiopia. J. Afr. Earth Sci. 44, 119–134.

Please cite this article in press as: Deroin, J.-P., et al. Integrating geologic and satellite radar data for mapping dome-and-basin patterns in the In Ouzzal Terrane, Western Hoggar, Algeria. J. Afr. Earth Sci. (2014), http://dx.doi.org/10.1016/j.jafrearsci.2014.03.015